A 12-lead ECG correlation network model exploring the inter-lead relationships

CHUANZHE ZHANG[1], JIAHAO LI[1], SHAOPENG PANG[1], FANGZHOU XU[2] and SHUWANG ZHOU[3]

[1] *School of Information and Automation Engineering, Qilu University of Technology(Shandong Academy of Sciences), Jinan, Shandong Province 250353, China*

[2] *School of Electronic and Information Engineering(Department of Physics), Qilu University of Technology (Shandong Academy of Science), Jinan, Shandong Province 250353, China*

[3] *Qilu University of Technology (Shandong Academy of Sciences), Shandong Artificial Intelligence Institute, Jinan 250014, China*

Abstract – The 12-lead Electrocardiogram (ECG) is widely used for automatic diagnosis of arrhythmia based on deep neural networks (DNN). In this paper, we use the 12-lead ECG dataset provided by the China Physiological Signal Challenge 2018 (CPSC2018), which contains 6877 samples and each sample contains 12-lead ECG records and corresponding reference labels. First, by statistical analysis of the results of 90 DNN models with $F_1 > 0.6$ published by CPSC2018, we found that almost all DNN models had high accuracy in identifying the Left bundle branch block (LBBB) even when the number of training samples for LBBB is severely insufficient. Second, through ablation studies, we found that the absence of the $7th$ lead V1 severely affected the diagnostic accuracy of many DNN models, where ablation studies were used to quantify the effect of the disappearance of a single lead on the F_1 of the DNN model. We aim to explain the above two special phenomena using complex network theory. A 12-lead ECG correlation network based on the inter-lead Pearson correlation coefficient is proposed, which allows us to observe the correlation between a single lead and others, and quantify the correlation strength of each lead through a projection process. We used the covariance method to quantify the consistency of the change trend for the average correlation strength of 12 leads between any two categories, and found that the mean values of the covariance for LBBB under the positive and negative 12-lead ECG correlation network were 0.01 and 0.07, respectively, much smaller than other categories. This uniqueness may explain from the perspective of complex networks why LBBB can be diagnosed accurately by almost all DNN models when its number of samples used for training is severely insufficient. Furthermore, we found that the correlation between the lead V1 and other leads was close to 0. This low correlation may make the information of the lead V1 significantly different from other leads, resulting in its important role in the automatic diagnosis of arrhythmia.

PACS: 87.85.Ng, 07.05.Mh, 89.75.Fb

Introduction . – The bioelectric process of the heart is closely related to the biochemical process of the heart tissue and the nervous system that controls the activity of the heart. Heart diseases caused by various pathological reasons are almost all related to the bioelectric activity of the heart. The ECG is a graphical display of the physiological activity signals of the heart. It reflects the process of electrical excitement generated and conducted in the cardiac conduction system. The 12-lead ECG is the most routine and important examination method for diagnosing arrhythmia [1].

Early research on the automatic diagnosis of arrhythmia was basically based on machine learning, including: signal pre-

processing [2], feature extraction [3], dimensionality reduction [4] and automatic classification [5]. Although machine learning has achieved good performance in the classification of arrhythmia, some potentially important features will be eliminated during the feature extraction process, which may affect the final classification efficiency. In recent years, DNN models have been widely used in the automatic diagnosis of arrhythmia due to their powerful feature extraction capabilities. Acharya et al. [6] used a 9-layer convolutional neural network (CNN) model to recognize and classify 5 arrhythmias, and achieved a classification accuracy of 94.03%. Tan et al. [7] connected CNN and long short term model in series to realize the automatic diagnosis of coronary artery disease. Singh et al. [8] compared the performance of three types of recurrent neural network models in the classification of arrhythmia, and obtained 85.4%, 82.5% and 88.1% accuracy rate, respectively. Hannun et al. [9] developed a DNN model that can classify 12 rhythms based on a single-lead ECG. Elola et al. [10] developed two DNN models for classifying pulse-generating rhythm and pulseless electrical activity using short single-lead ECG segments. Ribeiro et al. [11] demonstrated a DNN model trained on a dataset of more than 2 million mark checks and found that the model is superior to cardiologists in identifying 6 types of arrhythmias. Ullah et al. [12] converted a single-lead ECG into a two-dimensional spectral image as input for learning. Krasteva et al. [13] Optimized the hyperparameters of CNN model for detection of shockable and non-shockable rhythms, and to validate the best hyperparameter settings for short and long analysis durations. Jekova et al. [14] used an end-to-end CNN model named CNN3-CC-ECG, which was verified by them on an independent database OHCA and performed well. By automatic feature extraction, the model had a sensitivity of 89% for ventricular fibrillation, a specificity of 91.7% for non-shockable organised rhythms, and a specificity of 91.11% for asystole. Zhang et al. [15] proposed an interpretable DNN automatic diagnosis method based on 12-lead ECG.

The 1st China Physiological Signal Challenge (CPSC2018) [22] aims to encourage the development of algorithms for identification of rhythm abnormalities from 12-lead ECGs. The 12-lead ECG dataset used in this paper is from CPSC2018, in which the training set contains 6877 samples. Each sample contains 12-lead ECG records and the reference label, where label corresponds to 9 categories: Normal, Atrial fibrillation (AF), First-degree atrioventricular block (I-AVB), LBBB, Right bundle brunch block (RBBB), Premature atrial contraction (PAC), Premature ventricular contraction (PVC), ST-segment depression (STD) and ST-segment elevated (STE). The 12-lead ECG records are sampled as 500 Hz. More details of the dataset are shown in Tab. 1. 112 participating teams trained their DNN models using the 12-lead ECG dataset, and the output was labels corresponding to 9 categories. The CPSC2018 ran these DNN models on the test set, and announce the final results and rankings, as well as the code of 34 DNN models. Meanwhile, we obtained the results of 90 DNN models with $F_1 > 0.6$ published by CPSC2018, where F_1 [22] is an important indicator to quantify the performance of multi-classification tasks. The F_{1i} score of the ith arrhythmia is the harmonic average of precision $F_{\rm P}$ and recall $F_{\rm R}$,

$$F_{1i} = \frac{2(F_{\rm P} \times F_{\rm R})}{F_{\rm P} + F_{\rm R}}, \tag{1}$$

where $F_{\rm P} = {\rm TP}/({\rm TP} + {\rm FP})$ and $F_{\rm R} = {\rm TP}/({\rm TP} + {\rm FN})$, TP is the number of positive samples that are classified to be positive, FP is the number of negative samples that are classified to be positive, and FN is the number of positive samples that are classified to be negative. Then the F_1 is defined as:

$$F_1 = \frac{1}{9}\sum_{i=1}^{9} F_{1i}. \tag{2}$$

And the average and maximum F_{1i} of 90 DNN models in detecting the ith category are shown in Tab. 1.

Table 1: **12-lead ECG dataset and the F_{1i} measures of 90 DNN models for the normal rhythm and 8 arrhythmias.** For each type, we show the number of samples, the time length and the F_{1i} measures of 90 DNN models.

No.	Type	Number	Time length (s)		F_{1i} measure	
			Mean	Max	Mean	Max
1	Normal	918	15.43	64.00	0.657	0.765
2	AF	1098	15.04	74.00	0.883	0.940
3	I-AVB	704	14.38	74.00	0.825	0.900
4	LBBB	207	14.94	65.00	0.870	1.000
5	RBBB	1695	14.64	118.00	0.830	0.903
6	PAC	574	19.22	66.00	0.589	0.832
7	PVC	653	20.92	144.00	0.717	0.875
8	STD	826	15.51	138.00	0.672	0.800
9	STE	202	17.15	60.00	0.560	0.784

The F_{1i} of 90 DNN models and sample sizes for the normal rhythm and 8 arrhythmias are shown in Fig. 1. Statistics show that arrhythmias with high and concentrated F_{1i} values include AF and LBBB. It shows that many DNN models have outstanding performance for the diagnosis of AF and LBBB. However, the sample size of LBBB is much lower than AF and other arrhythmias(except for STE). As we all know, the more samples

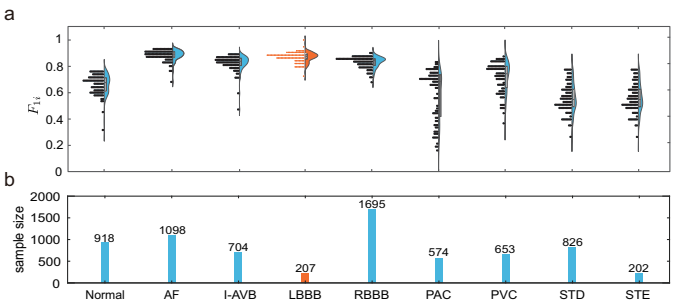

Fig. 1: **The F_{1i} of 90 DNN models and sample sizes for the normal rhythm and 8 arrhythmias.** (a) The distributions and probability densities of F_{1i} are described by semi-violin plots, where the F_{1i} of LBBB is high and the distribution is concentrated. (b) The sample sizes are depicted with dot-and-line plots, where the sample size of LBBB is the smallest compared to other arrhythmias (except for STE).

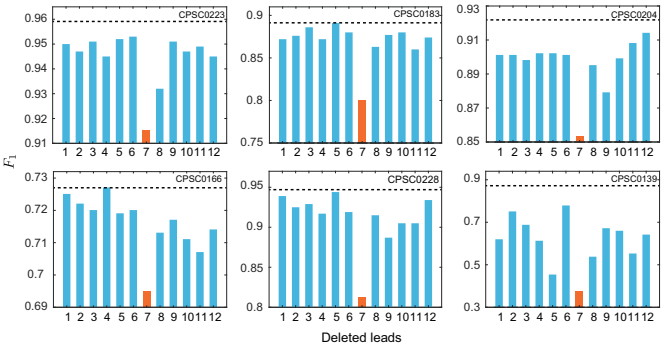

Fig. 2: **The F_1 of 6 DNN models with the information of a single lead deleted sequentially.** The F_1 of 6 DNN models after losing the information of a single lead in turn, where DNN models are from teams: 0223, 0183, 0204, 0166, 0228 and 0139 in CPSC2018. The original F_1 is represented as a virtual black line.

of an arrhythmia that can be used for training, the more accurately the DNN models can identify the arrhythmia. We found that the F_{14} of LBBB is still outstanding, although the sample size used for training has a huge disadvantage. This anomaly means that the 12-lead ECG corresponding to LBBB may be unusual in some respects.

In addition, we discovered another phenomenon through ablation studies. Specifically, limited by the operating environment and code (the code of some models downloaded is incomplete), we finally selected the 6 DNN models for ablation studies from the 34 DNN models whose codes were published. The input of all DNN models is the 12-lead ECG, and the output is the label corresponding to the normal rhythm and 8 arrhythmias. Each time, we delete the information of a single lead in the input and observed the predicted labels of the DNN models in this case. Based on the 6788 samples of CPSC2018, we obtained the F_1 of each DNN model after losing the information of a single lead in turn. As shown in Fig. 2, the F_1 of all DNN models drops significantly when the 7th lead V1 is missing. This suggests that the absence of V1 would severely impact the diagnostic accuracy of many DNN models.

This study aims to explain the two special phenomena from the perspective of complex networks [16, 17]: firstly, many DNN models had high accuracy in identifying the LBBB even when the number of training samples for LBBB is severely insufficient; secondly, the absence of the $7th$ lead V1 severely affected the diagnostic accuracy of many DNN models. The rest of this paper is organized as follows. A 12-lead ECG correlation network based on the Pearson correlation coefficient between leads is proposed in this paper, which allows us to observe the correlation between a single lead and other leads, and quantify the correlation strength of each lead through a projection process. Then, we provided an explanation for the above two peculiar phenomena from a complex network perspective based on 12-lead ECG correlation network. Conclusions are given at the end.

12-Lead ECG correlation network . – In order to investigate the above phenomena, we propose the 12-lead ECG correlation network based on the inter-lead Pearson correlation coefficient. Specifically, the 12-lead ECG correlation network $G(L, E)$ is an undirected weighted network with 12 nodes, where the node set $L = \{l_1, l_2..., l_{12}\}$ represents 12 leads and the edge weight between nodes is the correlation between leads. The Pearson correlation coefficient [23] is a classic method used to measure the linear correlation between two sets of data. Therefore, the correlation between the ith lead and jth lead is quantified by the Pearson correlation coefficient as

$$r_{ij} = \frac{\sum_{k=1}^{500T} (v_{ik} - \bar{v}_i)(v_{jk} - \bar{v}_j)}{\sqrt{\sum_{k=1}^{500T} (v_{ik} - \bar{v}_i)^2} \sqrt{\sum_{k=1}^{500T} (v_{jk} - \bar{v}_j)^2}}, \quad (3)$$

where v_{ik} is the voltage value of the ith lead at sampling point k, $500T$ is the total number of sampling points for a 12-lead ECG recording with T seconds, $\bar{v}_i = \frac{1}{500T} \sum_{k=1}^{500T} v_{ik}$ and $\bar{v}_j = \frac{1}{500T} \sum_{k=1}^{500T} v_{jk}$. $r_{ij} = 0$ means no linear correlation. $0 < r_{ij} \leq 1$ and $-1 \leq r_{ij} < 0$ represent positive and negative linear relationship, respectively. Note that the Pearson correlation coefficient between a lead and itself is $r_{ii} = 1$. A positive 12-lead ECG correlation network is established by retaining only positive correlations ($0 < r_{ij} \leq 1$) between leads. As shown in Fig. 3, we take 12 leads with $T = 2s$ as an example to show the establishment of the 12-lead ECG correlation network.

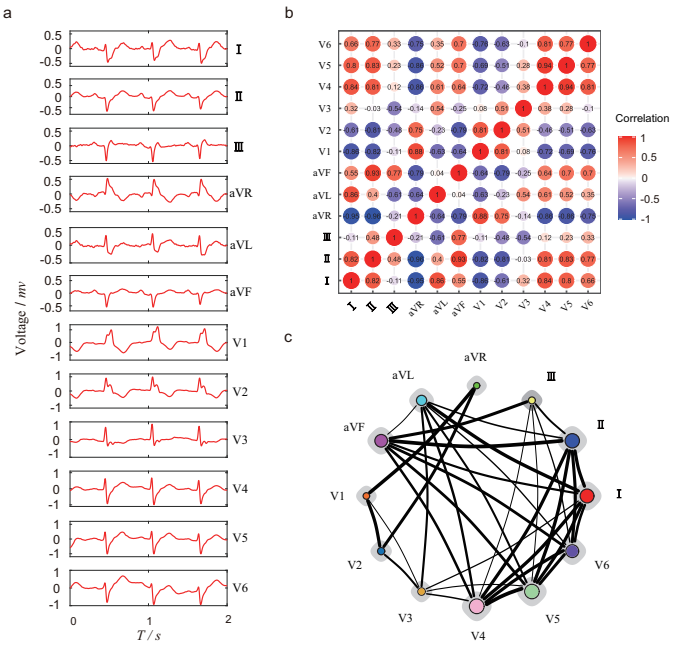

Fig. 3: **An example of establishing a 12-lead ECG correlation network.** (a) A 12-lead ECG data with $T = 2s$. (b) Correlations between 12 leads. (c) The positive 12-lead ECG correlation network $G(L, E)$ contains the node set $L = \{l_1, l_2..., l_{12}\}$ and the edge set E, where the edge weight is the positive Pearson correlation coefficient r_{ij} between two leads, and the edge weight is represented by the thickness of edge.

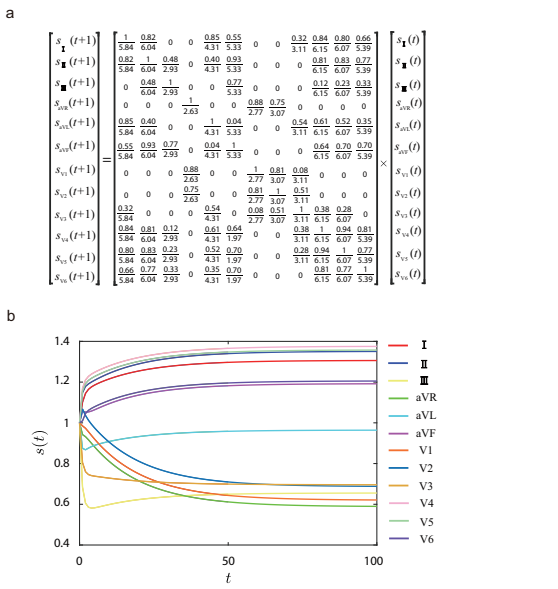

Fig. 4: **An example of the projection process.** (a) The projection matrix $W = \{w_{ij}\}_{12\times12}$ based on the positive 12-lead ECG correlation network in Fig. 3 and its projection process, where $\sum_{i=1}^{12} w_{ij} = 1$ for $\forall j$. (b) The initial resource vector $S(0)$ converges to the constant final resource vector $\bar{S}$ in a finite time, where the initial resource vector $S\,(0) = \{1, 1, ..., 1\}_{12\times1}$ is determined.

Based on the 12-lead ECG correlation network, we quantify the correlation strength of nodes inspired by the network projection process [18–20]. A positive 12-lead ECG correlation network can be represented by matrix $A = \{a_{ij}\}_{12\times12}$, where $a_{ii} = 1$ and $a_{ij} = r_{ij}$ if and only if leads l_i and l_j are positively correlated. Then we calculate the correlation strength of each node l_i through the projection process. Specifically, let the resource of the node l_i at time t be $s_i(t)$. At the next time $t+1$, the node l_i transfers its resource to neighbor nodes in proportion to the weight of all its connected edges, and receives resources from neighbor nodes at the same time. Therefore, the resource of node l_i at time $t + 1$ is

$$s_i\,(t+1) = \sum_{j=1}^{12} \frac{a_{ij} s_j\,(t)}{d(l_j)}, \tag{4}$$

where $d(l_j)$ is the degree of the node l_j. Let $w_{ij} = a_{ij}/d(l_j)$, the projection process can be written as

$$S\,(t+1) = W S\,(t)\,, \tag{5}$$

where $S\,(t) = \{s_1\,(t)\,, s_2\,(t)\,, ..., s_{12}\,(t)\}^T$ and $W = \{w_{ij}\}_{12\times12}$ is the projection matrix.

According to Ref. [19, 21], the matrix W^k will converge to a constant matrix for infinite k when $\sum_{i=1}^{12} w_{ij} = 1$ for $\forall j$ and the positive 12-lead ECG correlation network is the connected network. That is, when the initial resource vector $S(0)$ is determined, the final resource vector $\bar{S} = \lim_{k\to\infty} W^k S\,(0)$ is convergent, i.e., $\bar{S} = W\bar{S}$. Then the constant final resource vector can be calculated directly by

$$\bar{S} = \frac{\sum_{i=1}^{12} s_i(0)}{\sum_{i=1}^{12} p_{i1}} p_1, \tag{6}$$

where p_1 is the eigenvector corresponding to eigenvalue $\rho(W) = 1$ of the projection matrix W (See Appendix for details). As shown in Fig. 4, we continue to use the 12 leads with $T = 2s$ as an example to show the projection process of the 12-lead ECG correlation network, where the initial resource of each node l_i is $s_i(0) = 1$.

The projection process shows that when the initial resources of all nodes are the same, the constant final resource vector only depends on the network topology and edge weights. The more connected edges of a node l_i and the greater the weight of these edges, the higher the constant final resource that l_i can obtain. Therefore, the correlation strength of node l_i in the positive 12-lead ECG correlation network can be quantified by its final resource.

Results . – In order to study the anomaly of LBBB, we calculate the average correlation strength of the 12 leads for the normal rhythm and 8 arrhythmias. Let $C = \{c_1, c_2, ...c_9\}$

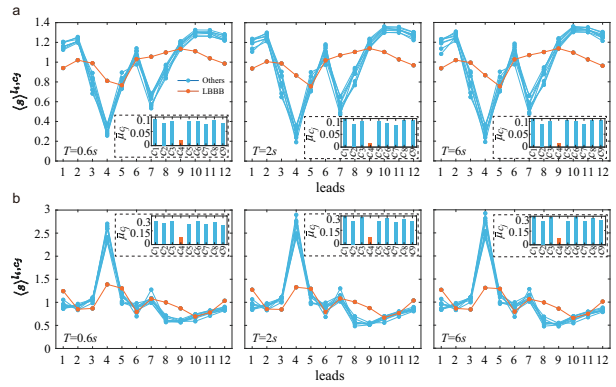

Fig. 5: **The average correlation strength of 12 leads.** The average correlation strength of 12 leads for the normal rhythm and 8 arrhythmias under the (a) positive and (b) negative 12-lead ECG correlation networks with $T = 0.6s$, $T = 2s$ and $T = 6s$, respectively. The mean value of the covariance for each category is shown in the dashed box, where the $\bar{\mu}_{c_4}$ of the $4th$ category (LBBB) is 0.02, 0.01, 0.01, 0.07, 0.07 and 0.07 under the (a) positive and (b) negative 12-lead ECG correlation networks with $T = 0.6s$, $T = 2s$ and $T = 6s$, respectively.

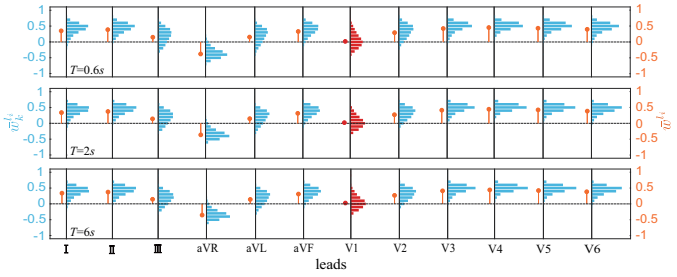

Fig. 6: **The distribution of average correlation.** The distribution of $\bar{w}_k^{l_i}$ is described by histogram and the mean $\bar{w}^{l_i}$ of 12 leads is described by semi-violin plot, where the $\bar{w}^{l_7}$ of the lead V1 is 0.01, 0.02 and 0.02 based on $T = 0.6s$, $T = 2s$ and $T = 6s$, respectively.

represents the normal rhythm and 8 arrhythmias in Tab. 1, and $G_k^{c_j}$ denotes the kth positive 12-lead ECG correlation network corresponding to category c_j, where $k = 1, 2, ..., n_{c_j}$ and n_{c_j} is the number of all positive 12-lead ECG correlation networks in category c_j. The average correlation strength corresponding to lead l_i under category c_j is

$$\langle s \rangle^{l_i,c_j} = \frac{1}{n_{c_j}} \sum_{k=1}^{n_{c_j}} \bar{s}_k^{l_i,c_j}, \tag{7}$$

where $\bar{s}_k^{l_i,c_j}$ is the correlation strength of node l_i in $G_k^{c_j}$. The consistency of the change trend for the average correlation strength of 12 leads between category c_j and category c_h $(c_h \neq c_j)$ is quantified by the covariance method as

$$\mu_{c_j,c_h} = \frac{1}{11} \sum_{i=1}^{12} \left(\langle s \rangle^{l_i,c_j} - \langle \bar{s} \rangle^{c_j} \right) \left(\langle s \rangle^{l_i,c_h} - \langle \bar{s} \rangle^{c_h} \right), \tag{8}$$

where $\langle \bar{s} \rangle^{c_j} = \frac{1}{12} \sum_{i=1} \langle s \rangle^{l_i,c_j}$. Further, we calculate the mean $\bar{\mu}_{c_j} = \frac{1}{8} \sum_{c_h \in C, c_h \neq c_j} \mu_{c_j,c_h}$ of each category. Fig. 5(a) shows the change trend of the average correlation strength of 12 leads in each category and the mean value of the covariance for each category. An important finding is that, except for LBBB, the change trend of the average correlation strength of 12 leads in all other categories is almost the same. The mean values of the covariance for LBBB is significantly lower than that of other categories, which supports the above findings. This shows that the topology and edge weight distribution of the positive 12-lead ECG correlation networks corresponding to LBBB are unique among the 9 categories. This uniqueness is likely to cause that, despite the insufficient number of samples used for training, the F_{14} corresponding to LBBB performed well. Moreover, we calculate the average correlation strength of the 12 leads and mean $\bar{\mu}_{c_j}$ for the normal rhythm and 8 arrhythmias based on the negative 12-lead ECG correlation network that only retains the negative correlation $(-1 \leq r_{ij} < 0)$ between the leads. Fig. 5(b) shows that the change trend of the average correlation strength of 12 leads corresponding to LBBB is still significantly different from other categories. This further illustrates the uniqueness of the topology and edge weight distribution of the 12-lead ECG correlation networks corresponding to LBBB. In order to eliminate the influence of the time length on the above results, we selected $T = 0.6s$ and $T = 6s$ as the control group. The results in Fig. 5 prove that the time length does not affect the final conclusion.

In summary, the most important finding is the uniqueness of the topology and edge weight distribution of the 12-lead ECG correlation networks corresponding to LBBB. This uniqueness may explain from the perspective of complex networks why many DNN models had high accuracy in identifying the LBBB even when the number of training samples for LBBB is severely insufficient.

In order to study the irreplaceability of the lead V1, we give the distribution of average correlation of 12 leads. Specifically, for a node l_i in a 12-lead ECG correlation network G_k, where $k = 1, 2, ..., n$ and n is the number of all 12-lead ECG correlation networks in 9 categories, we calculate its average correlation $\bar{w}_k^{l_i}$, i.e., the average weight of all connected edges of the node. Note that the value of each $\bar{w}_k^{l_i}$ is scattered in the range of $[-1, 1]$. We divide $[-1, 1]$ into 20 independent regions at an interval of 0.1, and calculate the proportion of $\bar{w}_k^{l_i}$ in each region. The results are shown in Fig. 6, a near-Poisson distribution with peak is presented in each lead. The aggregation of the $\bar{w}_k^{l_i}$ of all leads near their respective peaks indicates that their

distributions are homogeneous. We find that the $\bar{w}_k^{l_7}$ of the lead V1 is distributed near the peak $\bar{w} = 0$. This phenomenon does not occur in other leads and is unique to the lead V1. Furthermore, we calculate the mean $\bar{w}^{l_i} = \frac{1}{n}\sum_{k=1}^{n} \bar{w}_k^{l_i}$ of each lead. As shown in Fig. 6, there is a big difference in the $\bar{w}^{l_i}$ values of different leads. We guess that the higher the absolute value of $\bar{w}^{l_i}$, the stronger correlation between the lead l_i and other leads, which may cause the characteristics of the lead l_i to be more likely to be represented by other leads in the training of DNN models. In other words, the features contained in a lead can be obtained from other leads so that the absence of the lead does not seriously affect the diagnostic accuracy of DNN models. Conversely, $\bar{w}^{l_7} \approx 0$ indicates that the lead V1 has no positive or negative correlation with other leads, which may makes it irreplaceable in the training of DNN models. To eliminate the influence from the interception length, we selected $T = 0.6s$ and $T = 6s$ as the control group. The results in Fig. 6 prove that the interception length does not affect the final conclusion.

In summary, the most important finding is the correlation between a single lead and other leads may determines its role in the training of DNN models. When the positive and negative correlations between a single lead (such as the lead V1) and other leads are very low, the information of this lead is obviously different from other leads, causing its absence will seriously affect the prediction accuracy of the DNN model.

Conclusion . – Based on the framework of complex network, we studied the correlation between the 12 leads of ECG and its role in the diagnosis of arrhythmia. A 12-lead ECG correlation network is proposed to observe the correlation between leads. Then, based on the positive and negative 12-lead ECG correlation networks, we quantified the correlation strength of 12 leads through the projection process. We found that, except for LBBB, the change trend of the average correlation strength of 12 leads in all other categories is almost the same. This uniqueness may explains why LBBB can be diagnosed accurately by many DNN models when its number of samples used for training is insufficient. Furthermore, we found that, when the positive or negative correlations between a single lead (such as the lead V1) and other leads are very low, the information of this lead is obviously different from other leads, resulting in it playing an important role.

Our results not only offer a new perspective for exploring the correlation between 12 leads and their role in the diagnosis of arrhythmia, but also raise several questions. Future work directions include: exploring the topological characteristics of the 12-lead ECG, analyzing 12-lead ECG based on complex network, and improving the accuracy of arrhythmia diagnosis based on graph neural networks.

* * *

This work was supported by National Nature Science Foundation of China under Grant No. 61903208, Young doctorate Cooperation Fund Project of Qilu University of Technology (Shandong Academy of Sciences) under Grant No. 2019B-SHZ0014, Program for Youth Innovative Research Team in the University of Shandong Province in China under Grant No. 2019KJN010, Introduce Innovative Teams of 2021 "New High School 20 Items" Project under Grant No.2021GXRC071, and the Graduate Education and Teaching Reform Research Project of Qilu University of Technology in 2019 under Grant No. YJG19007.

Appendix. Correlation strength . – To prove Equation (6), we first introduce 3 lemmas [24, 25].

Lemma 1 *A graph is connected if and only if its adjacent matrix is irreducible.*

Lemma 2 *Let $A = A_{n\times n}$ and suppose that A is irreducible and nonnegative. Then*

(a) $\rho(A)$ is an eigenvalue of A;

(b) $\rho(A) > 0$;

(c) There is a positive vector p such that $Ap = \rho(A)p$;

(d) $\rho(A)$ is an algebraically (and hence geometrically) simple eigenvalue of A.

Lemma 3 *Let $A = A_{n\times n}$ and $A \geqslant 0$. When the row sums of A are fixed constant, then $\rho(A) = \|A\|_\infty$ is an eigenvalue of A. When the column sums of A are fixed constant, then $\rho(A) = \|A\|_1$ is an eigenvalue of A.*

Based on the above Lemmas, when $W > 0$ and $\sum_{i=1}^{n} w_{ij} = 1, \forall j$, $\rho(W) = 1$ is an eigenvalue of W and satisfies $Wp_1 = p_1$, where p_1 is a positive vector. Let invertible matrix $P = [p_1, p_2, ..., p_n]$ and $P^{-1} = [p_1^{*T}, p_2^{*T}, ..., p_n^{*T}]^T$, then

$$W' = P^{-1}WP = \begin{bmatrix} 1 & 0 \\ 0 & \overline{W}_{(n-1)\times(n-1)} \end{bmatrix}. \tag{9}$$

We have $W^T(p_1^*)^T = (p_1^*)^T$ since $P^{-1}W = W'P^{-1}$, where $(p_1^*)^T \in span(I_n)$ and $I_n = [1, 1, ..., 1]_{1\times n}^T$. Then $p_1^* p_1 = 1$ can obtain$p_1^* = \frac{1}{\sum_{i=1}^{n} p_{i1}}[1, 1, ..., 1]_{(1\times n)}$. The projection process can therefore be rewritten as

$$\widetilde{S} = \lim_{l\to\infty} P^{-1}W^l P\widetilde{S}(0) = \lim_{l\to\infty} \begin{bmatrix} 1 & 0 \\ 0 & \overline{W}^l_{(n-1)\times(n-1)} \end{bmatrix} \widetilde{S}(0), \tag{10}$$

where $\widetilde{S}(0) = P^{-1}S(0)$, $\widetilde{S} = P^{-1}\bar{S}$, $S(0) = \{s_1(0), s_2(0), ..., s_n(0)\}^T$ and $\bar{S} = \{\bar{s_1}, \bar{s_2}, ..., \bar{s_n}\}^T$ are the vector of initial and final resources, respectively. Since the spectral radius $\rho(\overline{W}) < 1$, the matrix $\lim_{l\to\infty} \overline{W}^l = 0$. Then

$$\bar{S} = p_1 p_1^* S(0) = \frac{\sum_{i=1}^n s_i(0)}{\sum_{i=1}^n p_{i1}} p_1, \tag{11}$$

where p_1 is the eigenvector corresponding to eigenvalue $\rho(W) = 1$ of the matrix W.

REFERENCES

[1] J. Schläpfer, H. J. Wellens, Computer-Interpreted Electrocardiograms: Benefits and Limitations, Journal of the American College of Cardiology 70 (9) (2017) 1183-1192.

[2] I. K. Daskalov, I. I. Christov, Electrocardiogram signal preprocessing for automatic detection of QRS boundaries, Medical Engineering & Physics 21(1) (1999) 37-44.

[3] R. G. Afkhami, G. Azarnia, M. A. Tinati, Cardiac arrhythmia classification using statistical and mixture modeling features of ECG signals, Pattern Recognition Letters 70 (2016) 45-51.

[4] J. S. Wang, W. C. Chiang, Y. L. Hsu, Y. Yang, ECG arrhythmia classification using a probabilistic neural network with a feature reduction method, Neurocomputing 116 (10) (2013) 38-45.

[5] P. D. Chazal, R. B. Reilly, A patient-adapting heartbeat classifier using ECG morphology and heartbeat interval features, IEEE Trans Biomed Eng 53 (2006) 2535-2543.

[6] U. R. Acharya, S. L. Oh, Y. Hagiwara, J. H. Tan, R. S. Tan, A deep convolutional neural network model to classify heartbeats, Computers in Biology & Medicine 89 (2017) 389-396.

[7] J. H. Tan, Y. Hagiwara, W. Pang, I. Lim, S. L. Oh, M. Adam, Application of stacked convolutional and long short-term memory network for accurate identification of cad ecg signals, Computers in Biology & Medicine 94 (2018) 19-26.

[8] S. Singh, S. K. Pandey, U. Pawar, R. R. Janghel, Classification of ecg arrhythmia using recurrent neural networks, Procedia Computer Science 132 (2018) 1290-1297.

[9] A. Y. Hannun, P. Rajpurkar, M. Haghpanahi, G. H. Tison, C. Bourn, M. P. Turakhia, Y. N. Andrew, Cardiologist-level arrhythmia detection and classification in ambulatory electrocardiograms using a deep neural network, Nature medicine 25 (2019) 65-69.

[10] A. Elola, E. Aramendi, U. Irusta, A. Picón, E. Alonso, P. Owens, A. Idris, Deep Neural Networks for ECG-Based Pulse Detection during Out-of-Hospital Cardiac Arrest, Entropy 21 (2019) 305.

[11] A. H. Ribeiro, M. H. Ribeiro, G. Paixo, D. M. Oliveira, P. R. Gomes, J. A. Canazart, M. P. Ferreira, Automatic diagnosis of the 12-lead ecg using a deep neural network, Nature Communications 11 (1) (2020) 1-9.

[12] A. Ullah, S. M. Anwar, M. Bilal, A. Al-Badarneh, R. M. Mehmood, Classification of arrhythmia by using deep learning with 2-d ecg spectral image representation, Remote Sensing 12 (10) (2020) 1685.

[13] V. Krasteva, S. Ménétré, J. P. Didon, I. Jekova, Fully Convolutional Deep Neural Networks with Optimized Hyperparameters for Detection of Shockable and Non-Shockable Rhythms, Sensors 20 (10) (2020) 202875.

[14] I. Jekova, V. Krasteva, Optimization of end-to-end convolutional neural networks for analysis of out-of-hospital cardiac arrest rhythms during cardiopulmonary resuscitation, Sensors 21 (2021) 4105.

[15] D. D. Zhang, S. Yang, X. H. Yuan, P. Zhang, Interpretable deep learning for automatic diagnosis of 12-lead electrocardiogram, Iscience 24 (4) (2021) 102373.

[16] S. Boccaletti, V. Latora, Y. Moreno, M. Chavez, D. U. Hwang, Complex networks: Structure and dynamics, Physics reports 424 (4-5) (2006) 175-308.

[17] R. Albert, A. Barabási, Statistical mechanics of complex networks, Reviews of Modern Physics 74 (1) (2002) 47-97.

[18] T. Zhou, J. Ren, M. Medo, Y. C. Zhang, Bipartite network projection and personal recommendation, Physical review E 76 (4) (2007) 046115.

[19] Q. Ou, Y. D. Jin, T. Zhou, B. H. Wang, B. Q. Yin, Power-law strength-degree correlation from resource-allocation dynamics on weighted networks, Physical Review E 75 (2) (2007) 021102.

[20] Y. L. Wang, T. Zhou, J. J. Shi, J. Wang, D. R. He, Empirical analysis of dependence between stations in Chinese railway network, Physica A: Statistical Mechanics and its Applications 388 (14) (2009) 2949-2955.

[21] C. Z. Zhang, S. P. Pang, Y. Hao, G. Z. Han, A fund-stock network projection model. Physica A: Statistical Mechanics and its Applications 566 (2021) 125630.

[22] http://2018.icbeb.org/Challenge.html

[23] J. Benesty, J. Chen, Y. Huang, I. Cohen, Pearson correlation coefficient, In Noise reduction in speech processing, Springer, Berlin, Heidelberg, 2009.

[24] J. N. Franklin, Matrix theory. Courier Corporation, 2012.

[25] W. H. Greub, Linear algebra, Springer Science & Business Media 2012.